

Analytical time-domain Green's functions for power-law media

James F. Kelly^{a)} and Robert J. McGough^{b)}

Department of Electrical and Computer Engineering, Michigan State University, East Lansing, Michigan 48824

Mark M. Meerschaert^{c)}

Department of Statistics and Probability, Michigan State University, East Lansing, Michigan 48824

(Received 29 April 2008; revised 19 July 2008; accepted 27 July 2008)

Frequency-dependent loss and dispersion are typically modeled with a power-law attenuation coefficient, where the power-law exponent ranges from 0 to 2. To facilitate analytical solution, a fractional partial differential equation is derived that exactly describes power-law attenuation and the Szabo wave equation [“Time domain wave-equations for lossy media obeying a frequency power-law,” *J. Acoust. Soc. Am.* **96**, 491–500 (1994)] is an approximation to this equation. This paper derives analytical time-domain Green's functions in power-law media for exponents in this range. To construct solutions, stable law probability distributions are utilized. For exponents equal to 0, 1/3, 1/2, 2/3, 3/2, and 2, the Green's function is expressed in terms of Dirac delta, exponential, Airy, hypergeometric, and Gaussian functions. For exponents strictly less than 1, the Green's functions are expressed as Fox functions and are causal. For exponents greater than or equal to 1, the Green's functions are expressed as Fox and Wright functions and are noncausal. However, numerical computations demonstrate that for observation points only one wavelength from the radiating source, the Green's function is effectively causal for power-law exponents greater than or equal to 1. The analytical time-domain Green's function is numerically verified against the material impulse response function, and the results demonstrate excellent agreement.

© 2008 Acoustical Society of America. [DOI: 10.1121/1.2977669]

PACS number(s): 43.35.Bf, 43.20.Hq, 43.20.Bi, 43.35.Mr [TDM]

Pages: 2861–2872

I. INTRODUCTION

The attenuation coefficient for biological tissue may be approximated by a power law¹ over a wide range of frequencies. Measured attenuation coefficients of soft tissue typically have linear or greater than linear dependence on frequency. For example, breast fat has a power-law exponent of $y=1.5$, while breast tissue ranges¹ from $y=1$ to $y=1.5$. This nonquadratic frequency-dependent loss conflicts with the classical thermoviscous attenuation and, by the Kramers–Kronig relations, predicts a frequency-dependent phase speed or dispersion. Mathematically, the power-law frequency dependence of the attenuation coefficient cannot be modeled with standard dissipative partial differential equations with integer-order derivatives such as the Stokes wave equation² or the telegrapher's equation.³ However, fractional partial differential equations (FPDEs) successfully capture this power-law frequency dependence.

Power-law attenuation has been incorporated in the time-domain via FPDEs, which add loss to the wave equation with a time-fractional derivative^{4–7} or a space-fractional derivative.^{8,9} Unlike loss models that utilize integer-order derivatives,^{10,11} these FPDEs support power-law attenuation coefficients for a range of noninteger exponents y . The Szabo wave equation is one such FPDE that interpolates between the telegrapher's equation ($y=0$) and the Blackstock equa-

tion ($y=2$), allowing a large range of lossy behavior to be encapsulated in an expression with two loss parameters: an attenuation coefficient and a power-law exponent.⁴ Frequency-domain formulations, based on the Kramers–Kronig relations^{12–14} between attenuation and dispersion, have also been proposed for linear frequency dependence¹⁵ and power-law dependence.^{16–18}

The bulk of the above work is numerical, which motivates additional analytical modeling of the combined effects of power-law loss and diffraction with Green's functions in the time-domain. Unfortunately, few closed-form solutions that describe the effects of dispersion in the time domain have been reported. To date, approximate closed-form Green's function solutions have only been provided for the special cases of $y=0$ (frequency-independent media) and $y=2$ (viscous media). In order to construct Green's functions for general power-law exponents y , stable law probability distributions, which have previously been used to study fractional diffusion, are required. These stable distributions facilitate analytical descriptions of power-law attenuation directly in the time domain.

The purpose of this paper is to derive analytical time-domain three dimensional (3D) Green's functions for power-law media for $0 < y < 2$ in terms of stable probability densities. These Green's functions are exact solutions for power-law media and approximate Green's functions to the Szabo wave equation. In Sec. II, the Szabo wave equation and the power-law wave equation corresponding to these solutions are formulated as FPDEs. 3D Green's functions are then calculated in Sec. III, allowing solutions to be obtained for frac-

^{a)}Electronic mail: kellyja8@msu.edu

^{b)}Electronic mail: mcgough@egr.msu.edu

^{c)}Electronic mail: mcubed@stt.msu.edu

tional power-law media in terms of the Fox H -function¹⁹ and the Wright function.²⁰ These functions have previously been used in the study of fractional diffusion,²¹ fractional relaxation,²² and fractional advection dispersion.⁹ In the special cases of $y=0, 1/3, 1/2, 2/3, 3/2,$ and $2,$ Green's function is expressed in terms of standard functions (Dirac delta, exponential, Airy, hypergeometric, and Gaussian functions). In the remaining cases, asymptotic expressions are provided. Numerical results and discussions of these results are provided in Secs. IV and V, respectively, followed by the conclusion in Sec. VI and the Appendix.

II. FPDE FORMULATIONS OF THE SZABO AND POWER-LAW WAVE EQUATIONS

A. Szabo wave equation

The Szabo wave equation⁴ approximates power-law media with an attenuation coefficient given by

$$\alpha(\omega) = \alpha_0 |\omega|^y. \quad (1)$$

The Szabo wave equation was originally derived as an integro-differential equation for fractional power-law media. Subsequently, Ref. 23 expressed the Szabo wave equation in terms of fractional derivatives, thereby allowing the machinery of fractional calculus to be utilized. For $y \neq 1,$ the Szabo wave equation is written as

$$\nabla^2 p - \frac{1}{c_0^2} \frac{\partial^2 p}{\partial t^2} - \frac{2\alpha_0}{c_0 \cos(\pi y/2)} \frac{\partial^{y+1} p}{\partial t^{y+1}} = 0, \quad (2)$$

where the third term accounts for dispersive loss. In the special cases of $y=0$ and $y=2,$ the fractional derivative term reduces to first and third temporal derivatives, respectively. For fractional $y,$ the third term is defined by the Riemann-Liouville fractional derivative defined in Appendix A.

For fractional $y,$ Eq. (2) is a FPDE that approximates lossy dispersive media satisfying a power-law. As discussed in Ref. 4, Eq. (2) is valid for $\alpha_0 \ll 1$ in the (a) high-frequency limit for $y < 1$ and (b) low-frequency limit for $y > 1.$ As shown below, a more general model for power-law media is obtained by including a higher-order temporal derivative. As in the case of the Stokes wave equation, the particle velocity and velocity potential also satisfy Eq. (2). From the definition of the fractional derivative given in Appendix A, Eq. (2) is also recognized as a singular integro-differential equation, where the fractional derivative term depends on the past history of the pressure $p(\mathbf{r}, t).$

B. Frequency-independent ($y=0$) and viscous ($y=2$) media

In the special cases of frequency-independent media ($y=0$) and viscous media ($y=2$), the Szabo wave equation reduces to well-known integer-order PDEs which are solved via standard methods. The $y=0$ case corresponds to the telegrapher's equation

$$\nabla^2 p - \frac{1}{c_\infty^2} \frac{\partial^2 p}{\partial t^2} - \frac{2\alpha_0}{c_\infty} \frac{\partial p}{\partial t} = 0, \quad (3)$$

which models one-dimensional (1D) damped string motion and electromagnetic wave propagation in conductive media. The reference frequency c_∞ is the phase speed in the limit of infinitely high frequency, and α_0 is the attenuation coefficient for $\omega=1.$ The 3D Green's function for Eq. (3) consists of two terms: an exponential attenuated spherical wave, which is localized at time $R/c_\infty,$ and a wake involving a modified Bessel function, which extends for infinite time. If α_0 is small, the modified Bessel function term is of order $\alpha_0^2,$ yielding the high-frequency approximation³

$$g(R, t) \approx u(t) e^{-\alpha_0 R} \frac{\delta(t - R/c_\infty)}{4\pi R} \quad (4)$$

where $u(t)$ is the Heaviside step function. Equation (4) is an attenuated spherical wave, which is localized in time and hence is nondispersive.

In the viscous case ($y=2$), the Szabo equation reduces to the Blackstock equation

$$\nabla^2 p - \frac{1}{c_z^2} \frac{\partial^2 p}{\partial t^2} + \frac{2\alpha_0}{c_z} \frac{\partial^3 p}{\partial t^3} = 0, \quad (5)$$

which models acoustic wave propagation in viscous media²⁴ under a plane wave approximation for small α_0 and for small frequencies. The reference frequency c_z is the phase speed in the limit of zero frequency. Since the spatial bandwidth of a wavefield is large near the source, Eq. (5) fails to capture the high-frequency content in the extreme near field of a radiator.^{2,24} The 3D Green's function of Eq. (5) is calculated via standard Fourier transform techniques, yielding

$$g(R, t) \approx \frac{1}{4\pi R} \sqrt{\frac{1}{4\pi R \alpha_0}} \exp\left(-\frac{(t - R/c_z)^2}{4R\alpha_0}\right), \quad (6)$$

which is an approximate solution to Eq. (5). Similar to the asymptotic solution to the Stokes wave equation,²⁵ Eq. (6) predicts Gaussian spreading of a spherical wave as the field radiates away from the source. However, Eq. (6) is non-causal, which means that Eq. (6) specifies nonzero field values for $t < 0.$ However, for α_0 small and R sufficiently large, Eq. (6) and the causal Green's function for the Stokes wave equation [see Eq. (3) in Ref. 26] are virtually indistinguishable, which is demonstrated numerically in Ref. 2 for the 1D case.

By utilizing the loss operator defined in Eq. (A2), the Szabo wave equation interpolates between the telegrapher's equation and the Blackstock equation. The telegrapher's equation is causal and hyperbolic, whereas the Blackstock equation is noncausal and parabolic. Mathematically, Eq. (2) is a second-order hyperbolic equation for $y < 1.$ For $y > 1,$ however, Eq. (2) becomes an order $y+1$ parabolic equation where high-frequency components propagate with infinite velocity. As $y \rightarrow 1^-$ in Eq. (2), $c_\infty \rightarrow \infty,$ and as $y \rightarrow 1^+$ in Eq. (2), $c_z \rightarrow \infty,$ which agrees with the transition between hyperbolic and parabolic behaviors at $y=1.$ Thus, the Szabo wave equation interpolates between the two different behaviors as the power-law exponent y varies from 0 to 2.

C. Power-law wave equation

As discussed in Ref. 4, Eq. (2) is an approximate model for wave propagation in a power-law medium for small values of α_0 . To facilitate the analytical solution of wave propagation in power-law media, a FPDE that exactly describes power-law attenuation for arbitrary α_0 is derived, and the Szabo wave equation is an approximation to this FPDE. This exact FPDE is then solved for a point source in space time, thereby yielding desired Green's function solution. Since both temporal and spatial Fourier transforms are utilized extensively throughout the derivation, the Fourier transform given by Eq. 3 in Ref. 4 is utilized throughout this paper. In order to derive the analytical time-domain Green's function solution, a power-law dispersion relationship relating wave-number k and angular frequency ω is required. This dispersion relationship should yield (1) a power-law attenuation coefficient and (2) a frequency-dependent phase speed. The power-law dispersion relationship that satisfies these requirements is

$$k = \frac{\omega}{c_0} - \frac{\alpha_0(-i)^{y+1}\omega^y}{\cos(\pi y/2)}, \quad (7)$$

for $\omega \geq 0$ and $k(-\omega) = k^*(\omega)$ to ensure real solutions. The imaginary part of Eq. (7) yields the power-law attenuation coefficient given by Eq. (1). The real part produces

$$\frac{1}{c(\omega)} = \frac{\text{Re } k(\omega)}{\omega} = \frac{1}{c_0} + \alpha_0 \tan\left(\frac{\pi y}{2}\right) |\omega|^{y-1}. \quad (8)$$

Letting c_1 denote the phase speed at $\omega_0 = 1$ yields the expression

$$\frac{1}{c(\omega)} = \frac{1}{c_1} + \alpha_0 \tan\left(\frac{\pi y}{2}\right) (|\omega|^{y-1} - 1), \quad (9)$$

which is valid for all $y \neq 1$. Equation (9) corresponds to the phase velocities computed via the Kramers–Kronig relations^{14,27} and the time-causal theory.¹³ In addition, Eq. (8) is in close agreement with the experimental dispersion data presented in Refs. 12–14 and 17. Thus, Eq. (2) supports the power-law attenuation and dispersion that is predicted by the Kramers–Kronig relationships and supported by experimental measurements.

In order to invert the wavenumber-frequency relationship into space time, the fourfold Fourier transform $\hat{P}(\mathbf{k}, \omega)$ of the time-domain pressure $p(\mathbf{r}, t)$ is multiplied by the dispersion relationship. Squaring both sides of Eq. (7) and multiplying by $\hat{P}(\mathbf{k}, \omega)$ yield

$$\left[-k^2 + \frac{\omega^2}{c_0^2} - \frac{2\alpha_0}{c_0 \cos(\pi y/2)} (-i\omega)^{y+1} - \frac{\alpha_0^2}{\cos^2(\pi y/2)} (-i\omega)^{2y} \right] \hat{P}(\mathbf{k}, \omega) = 0. \quad (10)$$

Performing an inverse spatial Fourier transform produces the power-law Helmholtz equation

$$\nabla^2 \hat{p} + \left[\frac{\omega^2}{c_0^2} - \frac{2\alpha_0}{c_0 \cos(\pi y/2)} (-i\omega)^{y+1} - \frac{\alpha_0^2}{\cos^2(\pi y/2)} (-i\omega)^{2y} \right] \hat{p} = 0. \quad (11)$$

Finally, performing an inverse temporal Fourier transform using Eq. (A3) yields the power-law FPDE

$$\nabla^2 p - \frac{1}{c_0^2} \frac{\partial^2 p}{\partial t^2} - \frac{2\alpha_0}{c_0 \cos(\pi y/2)} \frac{\partial^{y+1} p}{\partial t^{y+1}} - \frac{\alpha_0^2}{\cos^2(\pi y/2)} \frac{\partial^{2y} p}{\partial t^{2y}} = 0, \quad (12)$$

which satisfies the dispersion relationship, Eq. (7), exactly. For small α_0 , the fourth term in Eq. (12) is negligible, thus yielding the Szabo wave equation given by Eq. (2).

III. 3D GREEN'S FUNCTION

Time-domain 3D Green's functions for power-law media are derived in this section. These Green's functions are exact solutions to the power-law wave equation in Eq. (12) and approximate solutions to the Szabo wave equation in Eq. (2). Applying a point source at time $t=0$ to Eq. (12) and considering Green's function $g(R, t)$ yield

$$\nabla^2 g - \frac{1}{c_0^2} \frac{\partial^2 g}{\partial t^2} - \frac{2\alpha_0}{c_0 \cos(\pi y/2)} \frac{\partial^{y+1} g}{\partial t^{y+1}} - \frac{\alpha_0^2}{\cos^2(\pi y/2)} \frac{\partial^{2y} g}{\partial t^{2y}} = -\delta(\mathbf{R})\delta(t), \quad (13)$$

where \mathbf{R} is the relative displacement between the source and the observer and $R = |\mathbf{R}|$. Applying a temporal Fourier transform to Eq. (13) yields

$$\nabla^2 \hat{g} + k^2(\omega)\hat{g} = -\delta(\mathbf{R}), \quad (14)$$

where $k(\omega)$ is given by Eq. (7). The well-known Green's function for Eq. (14) is given by

$$\hat{g}(R, \omega) = \frac{e^{ik(\omega)R}}{4\pi R}. \quad (15)$$

Inserting Eq. (7) into Eq. (15) and grouping terms yield

$$\hat{g}(R, \omega) = \left[\frac{\exp(i\omega R/c_0)}{4\pi R} \right] [\exp(-\alpha_0 R(|\omega|^y - i \tan(\pi y/2)\omega|\omega|^{y-1}))], \quad (16)$$

where the first factor solves the lossless Helmholtz equation. The time-domain Green's function for $y \neq 1$ is recovered by applying an inverse Fourier transform and the convolution theorem, yielding

$$g(R, t) = \mathcal{F}^{-1}[\hat{g}(R, \omega)] = \left[\frac{\delta(t - R/c_0)}{4\pi R} \right] \mathcal{F}^{-1}[\exp(-\alpha_0 R(|\omega|^y - i \tan(\pi y/2)\omega|\omega|^{y-1}))], \quad (17)$$

which is expressed as a temporal convolution

$$g(R,t) = g_D(R,t) * g_L(R,t). \quad (18)$$

Within the framework of linear time-invariant filters, Eq. (18) combines the effects of dispersive loss and diffraction as a cascade of two system functions. The first factor in Eq. (18) is the Green's function for the lossless wave equation given by

$$g_D(R,t) = \frac{\delta(t - R/c_0)}{4\pi R}, \quad (19)$$

which is responsible for the effect of propagation and diffraction. The second term is a loss function defined via

$$g_L(R,t) = \mathcal{F}^{-1}[\exp(-\alpha_0 R(|\omega|^y - i \tan(\pi y/2)\omega)|\omega|^{y-1})]. \quad (20)$$

Interestingly, the inverse Fourier transform defined by Eq. (20) may be calculated in closed form using the machinery of stable distributions.²⁸ The expression within the square brackets in Eq. (20) is identified as the characteristic function of a stable distribution with index y , center 0, skewness 1, and scale $(R\alpha_0)^{1/y}$. The inverse transform given by Eq. (20) is then expressed concisely as

$$g_L(R,t) = \frac{1}{(\alpha_0 R)^{1/y}} \tilde{f}_y\left(\frac{t}{(\alpha_0 R)^{1/y}}\right), \quad (21)$$

where the function $\tilde{f}_y(t)$, which is independent of R and α_0 , is the maximally skewed stable distribution of index y with scale 1. This family of functions has been studied extensively.²⁹⁻³¹ Software is available for the computation of stable probability density functions (PDFs) and cumulative distribution functions³² based on formulas developed in Ref. 33. In the following analysis, an alternate parametrization $f_y(t)$ is defined via

$$f_y(t) = |\sec(\pi y/2)|^{1/y} \tilde{f}_y(|\sec(\pi y/2)|^{1/y} t), \quad (22)$$

in order to utilize existing expressions for the stable density $f_y(t)$. In the case of both sublinear power-law media ($y < 1$) and superlinear power-law media ($y > 1$), $f_y(t)$ possesses the following analytical properties: (1) $f_y(t) \geq 0$ for all t , (2) $f_y(t)$ is infinitely continuously differentiable (or smooth), (3) $f_y(t)$ is unimodal, and (4) $\int_{-\infty}^{\infty} f_y(t) dt = 1$. Although these properties are common to all maximally skewed stable distributions, the behavior of $f_y(t)$ differs for $y < 1$ and $y > 1$. Properties of these functions are studied in the following two subsections for sublinear ($y < 1$) and superlinear ($y > 1$) power-law media. The special case of $y = 1$ is discussed in Sec. III D.

Equation (18) is *approximate* Green's function, valid for small α_0 , for the Szabo wave equation given by Eq. (2). However, Eq. (18) is an *exact* solution to the power-law FPDE given by Eq. (12) for linear homogeneous media since the imaginary part of Eq. (7) exactly describes the power-law behavior that the Szabo wave equation approximates. Thus, analytical Green's function given by Eq. (18) is not restricted to small α_0 and large R .

A. Sublinear power-law media ($0 < y < 1$)

For the general case of $0 < y < 1$, $f_y(t)$ was first considered in Ref. 34 and later in Ref. 35 as an inverse Laplace transform. Rewriting Eq. (22) as a inverse Laplace transform yields

$$f_y(t) = \mathcal{L}^{-1}\{e^{-s^y}\} = \frac{1}{2\pi i} \int_L e^{-s^y} e^{st} ds, \quad (23)$$

where L is a contour in the left half plane. The notation is Eq. (23) was previously utilized in Ref. 36. The following analytic properties of $f_y(t)$ for $0 < y < 1$ are known:^{29,30} (1) $f_y(t)$ has support on $[0, \infty)$ and (2) as $t \rightarrow \infty$, $f_y(t) \sim t^{-y-1}$. The inverse Laplace transform defined by Eq. (23) is expressed in terms of the Fox H -function¹⁹ using formulas presented in Ref. 22. The Fox H -function, which is defined in terms of a contour integral by Eq. (B1), generalizes many of the special functions, such as Bessel, hypergeometric, and Mittag-Leffler.²⁰ Using Eq. (62) in Ref. 22, the fractional exponential possesses the representation

$$\exp(-s^y) = \frac{1}{y} H_{0,1}^{1,0}\left(s \left| \begin{matrix} (1,1) \\ (0,1/y) \end{matrix} \right. \right), \quad (24)$$

and the inverse Laplace transform is then calculated using Eq. (30) in Ref. 22, yielding

$$f_y(t) = \frac{1}{yt} H_{1,1}^{1,0}\left(\frac{1}{t} \left| \begin{matrix} (0,1) \\ (0,1/y) \end{matrix} \right. \right). \quad (25)$$

For $y = 0, 1/3, 1/2$, and $2/3$, Eq. (25) possesses the following exact representations:

$$f_0(t) = \delta(t), \quad (26a)$$

$$f_{1/3}(t) = \frac{u(t)}{(3t^4)^{1/3}} \text{Ai}\left[\frac{1}{(3t)^{1/3}}\right], \quad (26b)$$

$$f_{1/2}(t) = u(t) \frac{1}{2\sqrt{\pi t^{3/2}}} \exp\left(-\frac{1}{4t}\right), \quad (26c)$$

$$f_{2/3}(t) = u(t) \frac{2}{3\sqrt{\pi t^2}} \exp\left(-\frac{4}{27t^2}\right) {}_2F_0\left(\frac{1}{6}, -\frac{1}{6}; -\frac{27t^2}{4}\right), \quad (26d)$$

where $\text{Ai}(z)$ is the Airy function and ${}_2F_0(a, b; ; z)$ is the confluent hypergeometric function of the second kind.

For the general case, an asymptotic expression, valid for $t \ll 1$, is derived using the asymptotic form¹⁹ of $H_{1,1}^{1,0}(z)$. Alternatively, the inverse Laplace transform may be approximated via the method of steepest descents,³⁶ yielding

$$f_y(t) \approx u(t) \frac{A}{t^\nu} \exp\left(-\frac{B}{t^\mu}\right). \quad (27)$$

The coefficients A , B , ν , and λ depend only on y and are given by

$$A = \frac{y^{1/(2-2y)}}{\sqrt{2\pi(1-y)}}, \quad (28a)$$

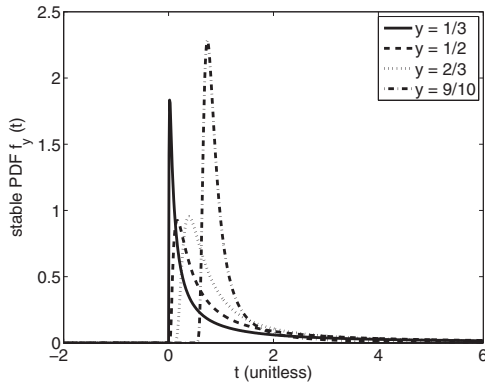


FIG. 1. Plots of maximally skewed stable PDFs $f_y(t)$ for four sublinear attenuation cases: $y=1/3$, $1/2$, $2/3$, and $9/10$. Equations (26a)–(26d) are evaluated for $y=1/3$, $1/2$, and $2/3$, while the $y=9/10$ case is evaluated with the STABLE toolbox (Ref. 32).

$$B = y^{1/(1-y)} \frac{1-y}{y}, \quad (28b)$$

$$\nu = \frac{2-y}{2-2y}, \quad (28c)$$

$$\mu = \frac{y}{1-y}. \quad (28d)$$

Equations (18), (27), and (28a)–(28d) provide a closed-form asymptotic approximation to the time-domain 3D Green's function for sublinear power-law media ($y < 1$). These equations exactly satisfy Eq. (26c) at all times t for $y=1/2$ and are valid for $y \neq 1/2$ when $t \ll 1$. For $y \approx 1/2$, Eq. (27) also provides an excellent approximation³⁷ for all values of t . For $t > 0$, f_y is infinitely continuously differentiable (or smooth); moreover, $f_y^{(n)}(t)=0$ as $t \rightarrow 0^+$ for all $n \geq 0$, implying strong causality.^{2,36} However, for $y \neq 1/2$ and $t \gg 1$, the asymptotic solution given by Eq. (27) decays exponentially for large times, while $f_y(t)$ decays algebraically. Therefore, for large t , the first term in the asymptotic series for Eq. (25) is utilized, yielding²⁹

$$\tilde{f}_y(t) \approx \frac{\sin(\pi y/2)\Gamma(y+1)}{\pi t^{y+1}}, \quad (29)$$

which indicates a slowly decaying tail.

To show the behavior of $f_y(t)$ for $0 < y < 1$, the PDFs for the sublinear attenuation cases $y=1/3$, $1/2$, $2/3$, and $9/10$ are displayed in Fig. 1. Since the ordinate $f_y(t)$ is a PDF, the abscissa t is unitless. The expressions given by Eqs. (26a)–(26d) are evaluated for $y=1/3$, $1/2$, and $2/3$, while the STABLE toolbox is utilized for $y=9/10$. In all of these cases, $f_y(t)$ is identically zero for $t < 0$ and smooth. As y increases from $1/3$ to $9/10$, the main plume spreads out, while the asymptotic decay accelerates from $t^{-4/3}$ to $t^{-19/10}$ due to the behavior predicted by Eq. (29).

As $y \rightarrow 0$, $f_y(t) \rightarrow \delta(t)$, while as $y \rightarrow 1^-$, $f_y(t) \rightarrow \delta(t-1)$. Thus, there is a delay incorporated into the stable distribution which accounts for the slower phase velocity in a dispersive medium. This delay is apparent in the asymptotic representation given by Eq. (27). For very small t , the argument of

the exponent in Eq. (27) is very large, causing $f_y(t)$ to approach zero. The delay t_d of $f_y(t)$ can be approximated by setting the exponential argument of Eq. (27) equal to unity, yielding $t_d \approx B^{1/\mu}$. Letting y vary from zero to 1, t_d is also seen to increase smoothly from zero to one.

B. Superlinear power-law media ($1 < y \leq 2$)

In superlinear power-law media, the qualitative behavior of the loss function $g_L(R, t)$ differs from that observed in sublinear power-law media. The maximally skewed stable distributions possess the additional analytical properties for $1 < y \leq 2$: (1) $f_y(t)$ has support on $(-\infty, \infty)$, (2) as $t \rightarrow \infty$, $f_y(t) \sim t^{-y-1}$ for $y < 2$, and (3) as $t \rightarrow -\infty$, $f_y(t)$ decays with exponential order. For $y > 1$, $f_y(t)$ is nonzero for all times t . Since the 3D Green's function is simply a delayed and scaled version of $f_y(t)$, the power-law Green's function $g(R, t)$ is nonzero for all t and is therefore noncausal for superlinear power-law media for all values of y such that $1 < y \leq 2$. Since $f_y(t)$ decays with exponential order as $t \rightarrow -\infty$, the solution is very small. This property, which was discussed by Szabo⁴ for the quadratic case ($y=2$), where $f_y(t)$ is Gaussian, is also true for all $1 < y \leq 2$ according to the stable law properties listed above.

The stable distribution $f_y(t)$ is evaluated in terms of the Fox H -function [see Eq. (2.13) in Ref. 38] via

$$f_y(t) = \frac{1}{y} H_{1,1}^{1,0} \left(-t \left| \begin{matrix} (1-1/y, 1/y) \\ (0, 1) \end{matrix} \right. \right), \quad (30)$$

where $1 < y \leq 2$. Equation (30) may be simplified in terms of the Wright function $\phi(a, b; z)$, yielding

$$f_y(t) = \frac{1}{y} \phi \left(-\frac{1}{y}, 1 - \frac{1}{y}; t \right), \quad (31)$$

which is a known solution of the time-fractional diffusion problem.³⁹ For the special cases of $y=3/2$ and $y=2$, Eq. (31) is expressed in terms of the confluent hypergeometric function of the second kind and a Gaussian, respectively:

$$f_{3/2}(t) = \begin{cases} \frac{3}{4\sqrt{\pi t}^{5/2}} {}_2F_0 \left(\frac{7}{6}, \frac{5}{6}; -; -\frac{27}{4t^3} \right) & \text{if } t > 0 \\ -\frac{2 \exp(4t^3/27)}{3\sqrt{\pi t}} {}_2F_0 \left(\frac{1}{6}, -\frac{1}{6}; -; \frac{27}{4t^3} \right) & \text{if } t < 0 \end{cases} \quad (32a)$$

$$f_2(t) = \frac{\exp(-t^2/4)}{\sqrt{4\pi}}. \quad (32b)$$

Note that the $y=2$ case in Eq. (32b) yields Eq. (6), which approximately solves the Blackstock equation²⁴ in Eq. (5).

Unlike the solution described earlier for sublinear power-law attenuation ($y < 1$), $f_y(t)$ is nonzero for all t . Therefore, three separate cases are considered: early time ($t \ll R/c_0$), late time ($t \gg R/c_0$), and times near the wavefront. To obtain an early-time estimate, Eq. (30) is expanded in a Taylor series.³⁸ If $t \ll R/c_0$, then $t_r \rightarrow \infty$, allowing an asymptotic representation of Eq. (30) to be utilized.³⁸

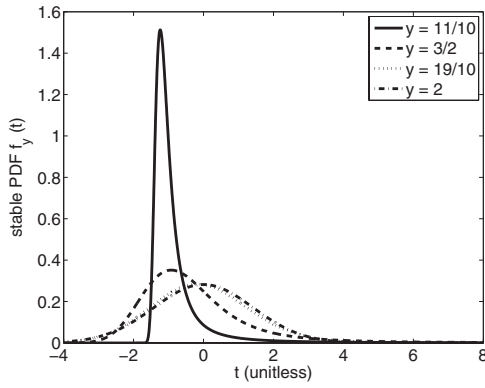


FIG. 2. Plots of maximally skewed stable PDFs $f_y(t)$ for four superlinear attenuation cases: $y=11/10$, $3/2$, $19/10$, and 2 . Equations (32a) and (32b) are evaluated for $y=3/2$ and 2 , while the $y=11/10$ and $19/10$ cases are evaluated with the STABLE toolbox (Ref. 32).

$$f_y(t) \approx A|t|^\nu \exp(-B|t|^\mu) \quad (33)$$

where

$$A = \frac{y^{-1/(2y-2)}}{\sqrt{2\pi(y-1)}}, \quad (34a)$$

$$B = y^{-y/(y-1)}(y-1), \quad (34b)$$

$$\nu = \frac{2-y}{2y-2}, \quad (34c)$$

$$\mu = \frac{y}{y-1}. \quad (34d)$$

For $y=2$, Eq. (33) reduces to $f_2(t)$ for all t , yielding the noncausal Blackstock solution. Equation (33) has the form of a “stretched exponential,” which is a characteristic of anomalous diffusion.⁴⁰ In other words, the early-time response of superlinear power-law media is characterized by fractional diffusive behavior. For large t , the asymptotic formula given by Eq. (29) is utilized.

Since Eq. (33) is nonzero for all t , power-law Green’s functions are noncausal for $1 < y \leq 2$. However, the rapid exponential decay for $t \ll R/c_0$ makes the solution very small for large negative times ($t \ll -1$). Thus, the noncausal nature of Green’s function for $1 < y \leq 2$ is not evident in numerical evaluations for small α_0 . From a physical perspective, the phase velocity becomes unbounded as frequency increases, implying that high-frequency components propagate infinitely fast. However, as noted in Ref. 2 for the special case of $y=2$, these high-frequency components experience high absorption and attenuate over a short distance, implying Green’s function $g(R, t) \ll 1$ for $t \ll R/c_0$.

To show the behavior of $f_y(t)$ for $1 < y \leq 2$, the stable PDFs for the superlinear power-law attenuation cases $y = 11/10$, $3/2$, $19/10$, and 2 are displayed in Fig. 2. The expressions given in Eqs. (32a) and (32b) are evaluated for $y = 3/2$ and 2 , while the STABLE toolbox³² is utilized for $y = 11/10$ and $19/10$. In all cases, $f_y(t)$ is nonzero for all t and smooth. For $y = 11/10$, $f_y(t)$ is skewed to the right and decays very rapidly for $t < -1$. As y increases from $11/10$ to 2 , the

PDF becomes increasingly symmetric, eventually converging to a Gaussian. Although $y=11/10$, $3/2$, and $19/10$ decay like t^{-y-1} , $y=2$ decays much more rapidly.

C. Linear power-law media ($y=1$)

The FPDE formulations of both the Szabo wave equation, given by Eq. (2), and the power-law wave equation, given by Eq. (12), break down as $y \rightarrow 1$ since $\cos(\pi y/2) \rightarrow 0$ in the denominator. To circumvent this problem, the frequency-domain solution at a reference frequency $\omega_0=1$ is considered. The phase velocity is computed by taking the limit of Eq. (9) as $y \rightarrow 1$. Without loss of generality, let y approach one from the right. Defining $y=1+\epsilon$ and letting $\epsilon \rightarrow 0$, then

$$\begin{aligned} \frac{1}{c(\omega)} &= \frac{1}{c_1} + \alpha_0 \tan(\pi(1+\epsilon)/2)(|\omega|^\epsilon - 1) \\ &= \frac{1}{c_1} - \alpha_0 \frac{|\omega|^\epsilon - 1}{\tan(\pi\epsilon/2)} \rightarrow \frac{1}{c_1} + \frac{2\alpha_0}{\pi\epsilon} (|\omega|^\epsilon - 1), \end{aligned} \quad (35)$$

where the limit $\tan z \rightarrow z$ is used in the last line. To finish the computation, the following limit is invoked:⁴¹

$$\frac{w^\gamma - 1}{\gamma} \rightarrow \ln(w), \quad (36)$$

yielding

$$\frac{1}{c(\omega)} = \frac{1}{c_1} - \frac{2\alpha_0}{\pi} \ln|\omega|. \quad (37)$$

Equation (37) is identical to the Hilbert dispersive model derived in Ref. 15 and the Kramers–Kronig relation given by Eq. (13) in Ref. 14. Combining Eqs. (1) and (37) yields a dispersion relationship between the wavenumber k (spatial frequency) and the temporal frequency ω :

$$k(\omega) = i\alpha_0|\omega| + \frac{\omega}{c_1} - \frac{2}{\pi}\alpha_0\omega \ln|\omega|. \quad (38)$$

The 3D time-domain Green’s function is computed by inserting Eq. (38) into the frequency-domain Green’s function given by Eq. (15) and assigning the delay term ω/c_1 to $\hat{g}_D(R, \omega)$. Inverse Fourier transforming this product of diffraction and loss factors yields Eq. (18) with a loss function

$$g_L(R, t) = \mathcal{F}^{-1} \left\{ \exp \left[-\alpha_0 R |\omega| \left(1 + \frac{2i \operatorname{sgn}(\omega) \ln|\omega|}{\pi} \right) \right] \right\}, \quad (39)$$

where the signum function $\operatorname{sgn}(\omega)$ is introduced to enforce conjugate symmetry. Equation (39) is recognized as a stable distribution with index 1, center 0, skewness 1, and scale $\alpha_0 R$ using the parametrization in Ref. 28. Thus, the inverse Fourier transform is expressed as

$$g_L(R, t) = \frac{1}{\alpha_0 R} \tilde{f}_1 \left(\frac{t}{\alpha_0 R} \right), \quad (40)$$

where $\tilde{f}_1(t)$ is the inverse Fourier transform of Eq. (39) with $\alpha_0 R=1$. Carrying out the transform by integrating over the negative and positive frequencies and expressing the cosine in terms of complex exponentials yield

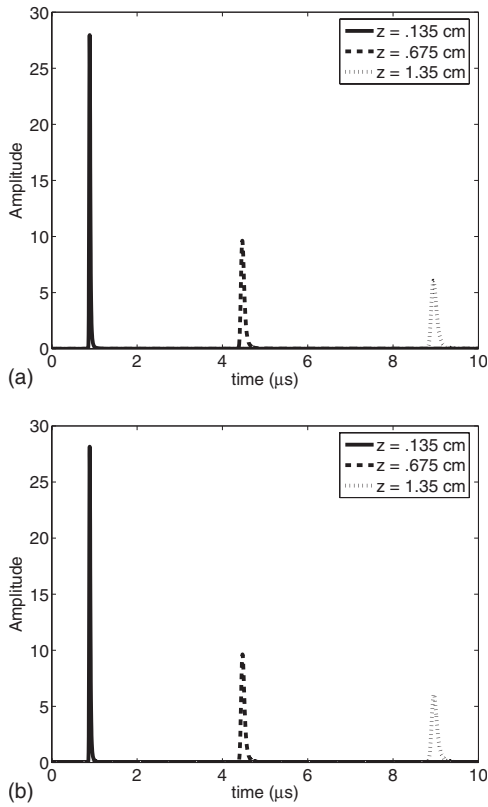


FIG. 3. Comparison of 3D Green's functions using (a) the MIRF approach and (b) the analytical Green's function approach given by Eq. (18). Green's functions are displayed at three different depths with $\gamma=1.5$, $c_0=0.15$ cm/ μ s, and $\alpha_0=0.1151$ Np/MHz^{1.5}/cm.

$$\tilde{f}_1(t) = \frac{1}{\pi} \int_0^\infty \exp(-\omega) \cos \left[\omega t + \frac{2}{\pi} \omega \ln \omega \right] d\omega. \quad (41)$$

Although $\tilde{f}_1(t)$ cannot be expressed in terms of the Fox or Wright functions, this expression is computable using the STABLE toolbox.³² Moreover, $\tilde{f}_1(t)$ has the same analytical properties as the superlinear power-law solutions shown earlier, including smoothness and exponential decay as $t \rightarrow -\infty$. Since $f_y(t)$ is nonzero for all t , the power-law Green's function is noncausal for $\gamma=1$. For $t \gg 1$, the asymptotic behavior of $\tilde{f}_1(t)$ is given by Eq. (29), which estimates the tail of the Green's function.

IV. NUMERICAL RESULTS

To numerically verify the analytical results presented above, the analytical Green's function was compared to the material impulse response function (MIRF) approach developed in Ref. 16. In Fig. 3(a), the 3D Green's function is computed in a power-law medium with parameters $\gamma=1.5$, $c_0=0.15$ cm/ μ s, and $\alpha_0=0.1151$ Np/MHz^{1.5}/cm using the analytical formula in Eq. (18). In Fig. 3(b), the inverse Fourier transform defined by Eq. (20) was calculated numerically via an inverse fast Fourier transform (FFT). The two panels demonstrate excellent agreement. For power-law exponents $\gamma=1/3$, $1/2$, $2/3$, $3/2$, and 2 , the function $f_y(t)$ is represented in terms of the Airy, hypergeometric, exponential, and Gaussian functions. Equations (26a), (26b), (32a),

and (32b) are evaluated numerically using the GNU Scientific Library.⁴² For other values of γ , the function $f_y(t)$ is represented as a maximally skewed stable distribution computed using the software package STABLE,³² which is a general-purpose software for analyzing stable distributions. The results of STABLE have been independently verified using codes developed by Robinson⁴³ and a combination of asymptotic expressions, power series, and inverse power series. All demonstrate excellent numerical agreement. Transient fields are then evaluated using FFT-based convolutions.

Figure 4 shows the 3D power-law Green's function for $\gamma=1/2$, $3/2$, and 2 for $\alpha_0=0.05$ mm⁻¹ MHz^{- γ} . The Green's functions are shown as functions of the radial coordinate R for times $t=20$, 30 , 40 , and 50 μ s in order to emphasize the spatial distribution of acoustic energy in power-law media. The qualitative properties of sublinear power-law media ($\gamma=0.5$), superlinear power-law media ($\gamma=1.5$), and viscous media ($\gamma=2$) are displayed in these plots. In these figures, the impulsive excitation has been stretched and smoothed by the filtering effect of the medium. The Green's function for sublinear power-law media ($\gamma=0.5$) has a sharp wavefront at $R=c_0t$, where the field is identically zero to the right of this wavefront. Neither the superlinear power-law attenuation Green's function nor the viscous Green's function has this sharp wavefront. In the $\gamma=1.5$ case, most of the energy is located in the slowly decaying tail of the Green's function, whereas in the viscous case ($\gamma=2$), energy is symmetrically distributed about the location $R=c_0t$.

As time evolves in Figure 4, the peak amplitudes of all three of the Green's functions decrease, thus accounting for the transfer of acoustic energy into random thermal energy within the intervening medium. In the $\gamma=0.5$ and $\gamma=1.5$ cases, the duration of the Green's function increases, which is a consequence of the heavy tail behavior predicted by the asymptotic expression in Eq. (29). In the viscous case ($\gamma=2$), spreading of the main plume occurs, although the Green's function is more localized relative to the fractional cases due to the rapid decay of the Green's function for large times. The absence of a slowly decaying tail is a consequence of the minimal dispersion associated with viscous and thermo-viscous loss.

To explore the effect of frequency-dependent attenuation on broadband pulse propagation, the velocity potential due to a point source at the origin was computed by convolving Eq. (18) with the pulse^{44,45}

$$v(t) = A_0 t^3 \exp(-\beta t) \sin(2\pi f_0 t) \text{rect} \left(\frac{t}{W} \right). \quad (42)$$

The following simulations utilize the center frequency $f_0=2.5$ MHz, pulse length $W=1.2$ μ s, damping factor $\beta=9.3750$ μ s⁻¹, and a normalization factor of $A_0=616.3$ mm/ μ s. Two examples of velocity potential calculations are shown in two power-law media using parameters from Ref. 1: (1) a fat-like medium with $\gamma=1.5$, $c_0=1.432$ mm/ μ s, and $\alpha_0=0.086$ Np/MHz^{1.5}/cm and (2) a liver-like medium with $\gamma=1.139$, $c_0=1.569$ mm/ μ s, and $\alpha_0=0.0459$ Np/MHz^{1.139}/cm.

Figure 5 displays the velocity potential as a function of time t at radial distances 10, 25, 50, and 100 mm to show the

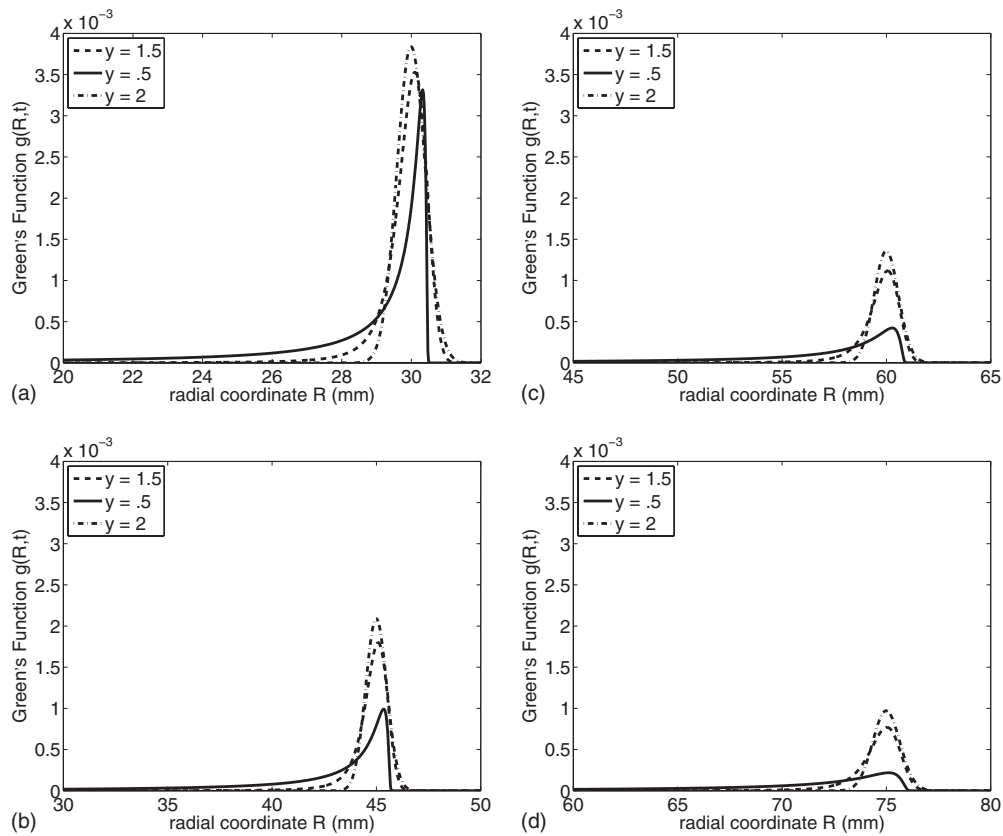


FIG. 4. Snapshots of the 3D power-law Green's function for $y=0.5, 1.5,$ and 2.0 for $\alpha_0=0.05 \text{ mm}^{-1} \text{ MHz}^{-y}$. Snapshots of the Green's function are shown for $t=20, 30, 40,$ and $50 \mu\text{s}$.

effect of dispersion on the pulse shape. As R increases in Fig. 5, several qualitative features become evident. First, the pulse experiences rapid attenuation due to the combined effects of loss and spherical spreading. Second, the pulse changes shape due to the more rapid attenuation of the high-frequency components. In other words, the spectrum of the pulse experiences a frequency downshift. There are significant differences between the fat-like medium and the liver-like medium. The fat-like medium is more dissipative; therefore, greater attenuation and greater frequency downshifts are observed for large depths ($R=100 \text{ mm}$). Although the liver-like medium is increasingly attenuated as the propagation distance increases, there is little change in the pulse shape. The pulse distortion in the fat-like medium indicates that the effects of dispersion become significant for large depths, which is consistent with the conclusion reached in Ref. 27.

V. DISCUSSION

A. Causality and the superlinear attenuation paradox

In Ref. 4, the “quadratic loss paradox” associated with the 1D solution of the Blackstock equation given by Eq. (5) is presented. In the discussion of Sec. VII of Ref. 4, Szabo notes that the 1D solution is noncausal yet provides an excellent approximation to the thermoviscous wave equation for small values of $\epsilon=\alpha_0 c_0 |\omega|^{y-1}$, where ω is the upper frequency limit. Szabo’s analysis is applied to three dimensions for superlinear power-law media ($y > 1$).

By letting $\hat{R}=R/\lambda$, where λ is the wavelength associated with ω , the ratio of Green’s function at time $t=0$ to the peak value is given by

$$\eta = \frac{f_y(-R/c_0/(\alpha_0 R)^{1/y})}{\max f_y(z)} = \frac{f_y(-\hat{R}^{1-1/y}\chi)}{\max f_y(z)} \quad (43)$$

where $\chi = |\sec(\pi y/2)|^{1/y}/(c_0 \alpha_0^{1/y})$. Letting the normalized distance $\hat{R}=1$ in Eq. (43) yields the upper limit $20 \log_{10} \eta < -136 \text{ dB}$ for $1 < y \leq 2$. However, values of η are typically much smaller than this upper limit. For instance, for $y=1.5$, $20 \log_{10} \eta < -360 \text{ dB}$. Similar computations for other $y \geq 1$ demonstrate that for observation points only one wavelength from the radiating source, Eq. (18) is effectively causal for all $0 < y \leq 2$.

B. Physical interpretation and application to ultrasonic imaging

Unlike the Green’s function for lossless media, the Green’s function for power-law media is not localized in space. Rather, the energy radiated by a point source is smeared out over a wide volume. For viscous media ($y=2$), the Green’s function, given by a shifted and scaled Gaussian, decays rapidly for observation points distant from $c_0 R$. For $y < 2$, however, the Green’s function decays as an inverse power of distance for observation points between the origin and R . This slow decay is interpreted as the gradual relaxation of the medium after the initial wavefront has passed. As time evolves from $t=20 \mu\text{s}$ to $t=50 \mu\text{s}$ in Fig. 4, the tail of

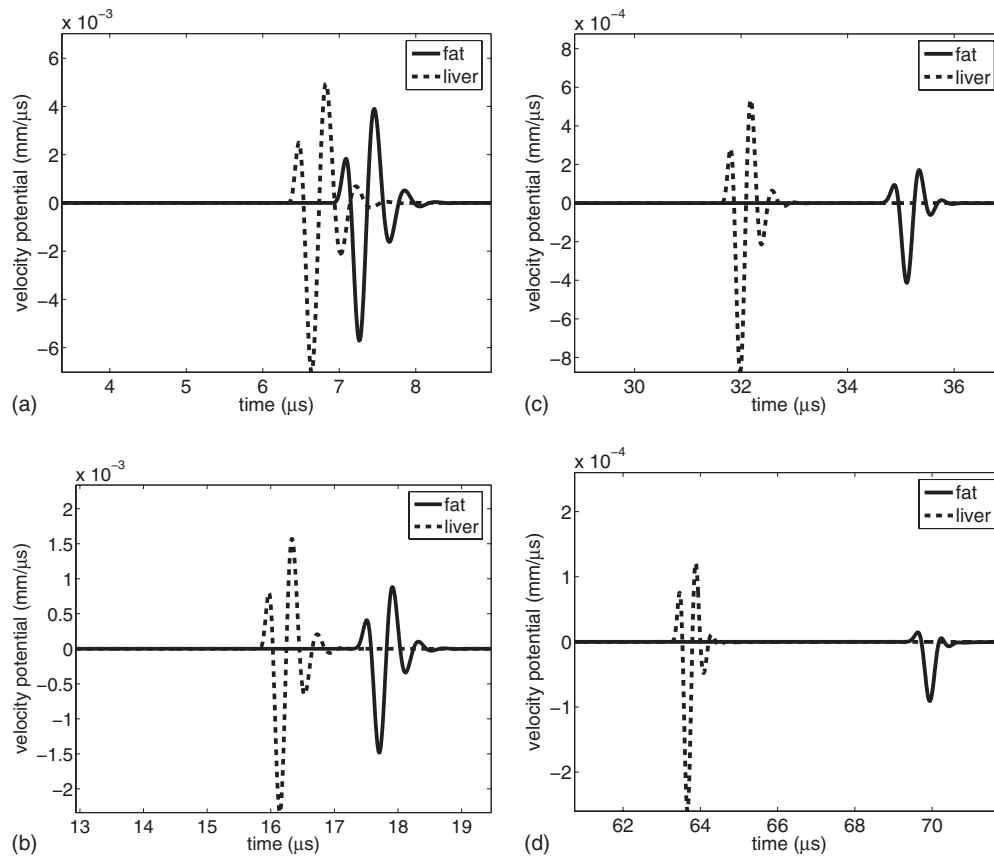


FIG. 5. Velocity potential produced by a point source excited by a broadband pulse defined by Eq. (42) in two power-law media: (1) a fat-like medium with $y=1.5$, $c_0=1.432$ mm/ μ s, and $\alpha_0=0.086$ Np/MHz^{1.5}/cm and (2) a liver-like medium with $y=1.139$, $c_0=1.569$ mm/ μ s, and $\alpha_0=0.0459$ Np/MHz^{1.139}/cm. The velocity potential is displayed at radial distances 10, 25, 50, and 100 mm.

the Green's function increases in both amplitude and duration, indicating that acoustic energy is being transferred from an organized spherical wavefront to a slowly decaying wake. Since this slow decay is not evident in the viscous case ($y=2$), a mechanism other than viscous dissipation (such as scattering by subwavelength structures) may be responsible for the observed wake.

Understanding the effect of attenuation on ultrasonic fields is important in *B*-mode image synthesis⁴⁶ and full-wave simulations in heterogeneous media.⁴⁷ Although the predicted change in phase velocity in most biological tissue is small,¹² the effects of dispersion accumulate with propagation distance and may alter pulse shape over acoustically large distances.²⁷ For instance, the change in phase velocity in the fat-like medium over the bandwidth of the pulse is less than 3 m/s, yet the incident pulse undergoes a significant frequency downshift at a depth of $R=100$ mm.

The 3D power-law Green's functions derived in Sec. III facilitate the study of 3D sound beams in dispersive power-law media. In particular, the impulse response produced by baffled circular and rectangular pistons may be constructed by integrating power-law Green's function over the radiating aperture. Specifically, the methodology developed in Ref. 26 for circular apertures in viscous media and Ref. 48 for rectangular apertures in viscous media may be extended to power-law dispersive media by utilizing the analytical Green's functions derived above. Since the power-law Green's function is efficiently evaluated using the STABLE

toolbox,³² the analytical expressions presented here may be used to either validate fields generated by dispersive full-wave linear solvers⁷ or construct efficient single-scattering codes based on the Born approximation. Therefore, the analytical tools developed in this paper may further the understanding of the influence of dispersive loss on ultrasonic scattering and image formation.

Figure 5 provides an example of one such evaluation. For large depths ($R=50$ mm and $R=100$ mm), the distortion of the pulse is clearly evident in the fat-like medium but much less apparent in the liver-like medium. In fat, attenuation increases with frequency at a greater rate ($y=1.5$) than in liver ($y=1.139$), yielding a larger frequency downshift. Since attenuation and dispersion increase with frequency, increasing the center frequency f_0 of the pulse will increase both the absolute magnitude of frequency downshift and time delay, thereby degrading the ultrasound image in a diagnostic application. To address this problem, the analytical Green's functions presented in this paper may be used to select and evaluate pulse sequences for different imaging applications.

C. Comparison to frequency-domain models

To further validate the power-law Green's function, the Green's function for linear with frequency attenuation ($y=1$) was compared to the dispersive tissue model presented in Ref. 15, which incorporates a logarithmic frequency-

dependent phase delay that is equivalent to Eq. (37). Since Ref. 15 utilizes a 1D model, the $1/(4\pi R)$ factor in the power-law Green's function was omitted from this evaluation. The impulse response associated with the dispersive tissue model shown in Fig. 2 of Ref. 15 was then reproduced by evaluating Eq. (40) using the STABLE toolbox at times t retarded by a bulk delay given by $\tau_b=1/c_1=6.67 \mu\text{s}/\text{cm}$. The minimum phase τ_m presented in Ref. 15 is not required in the evaluation since this additional delay is incorporated into the stable density $\tilde{f}_1(t)$.

The analytical time-domain Green's functions presented in this paper may serve as references for calculations in a dispersive tissue model. These analytical models may prove advantageous relative to the frequency-domain models proposed in Refs. 15, 16, and 27, which require the evaluation of numerical inverse Fourier transforms. To expedite these inverse transforms, FFTs are utilized, which require (1) uniform discretization in time and (2) adequate sampling of $\hat{g}(R, \omega)$ in the temporal frequency domain. In contrast, the time-domain power-law Green's functions presented above are not limited by these two requirements. These Green's functions may be evaluated on a nonuniform grid of time samples without sacrificing efficiency. For example, these power-law Green's functions may be used to validate finite difference time domain codes which use nonuniform time stepping. In addition, the error tolerance associated with evaluating $f_y(t)$ via the STABLE toolbox is user specified,³² thus making these analytical Green functions an ideal reference for MRF and dispersive tissue model calculations.

D. Alternate fractional models

FPDEs have previously been utilized in hydrogeology to model advection due to microheterogeneity.^{9,49} These FPDE models utilize a 1D advection-dispersion equation to capture the dispersion in heterogeneous aquifers. Like the solutions to the power-law wave equation, the solutions to the advection-dispersion equation are translated and scaled stable distributions, thus suggesting a connection between the hydrogeologic and ultrasonic models. Also, sound speed heterogeneity has been proposed as a mechanism for attenuation in marine sediments.⁵⁰ Since one possible mechanism for ultrasonic absorption is Class 0 scattering due to microheterogeneity,⁵¹ the power-law wave equation may approximate scattering due to heterogeneity at the macromolecular level. The explicit connection between macromolecular scattering and power-law attenuation requires advanced mathematical tools such as homogenization theory and/or subordinated random processes.³⁰

Alternate FPDE models for power-law attenuation have been reported, including models by Chen-Holm⁸ and Wismer.⁷ The Chen-Holm model utilizes a space-fractional derivative of order y , while the Wismer model utilizes a fractional time derivative of order $y-1$. Both the Chen-Holm and the Wismer models support power-law attenuation with exponent y in the zero-frequency limit, which is desirable for biomedical applications. Analysis of these models using the mathematical tools developed in this paper is an intended topic of future research.

VI. CONCLUSION

3D Green's functions in power-law media have been analytically computed in the time domain using the tools of fractional calculus. This paper shows that Green's functions for a medium with an attenuation coefficient given by Eq. (1) are maximally skewed stable distributions, shifted by a delay R/c_0 , scaled by $(\alpha_0 R)^{1/y}$, and multiplied by a spherical diffraction factor of $1/(4\pi R)$. Mathematically, power law Green's functions are represented by a transient spherical wave, which embodies the diffractive process, convolved with a loss function $g_L(R, t)$, which embodies both the attenuation and dispersion of the medium. Physically, therefore, the solutions to the power-law wave equation are represented as the linear coupling of diffraction and dispersive loss. The time-domain power-law Green's functions presented here are exact solutions to the power-law wave equation in Eq. (12) and approximate solutions to the Szabo wave equation given by Eq. (2).

By solving for the time-domain power-law Green's function with the machinery of stable distributions, efficient numerical evaluation is available via the STABLE toolbox.³² For all $y < 1$, these Green's functions are expressed in terms of Fox H -functions, while for $y > 1$, the Green's function is expressed in terms of the H function and Wright functions. For $y=0, 1/3, 1/2, 2/3, 3/2$, and 2 , the Green's function solutions are expressed in terms of widely known special functions. The analytical Green's function was numerically verified against the MRF result¹⁶ and Hilbert dispersive model,¹⁵ and example fields were computed. The results show that power-law Green's function is causal for $y < 1$ and noncausal for $1 \leq y \leq 2$. Despite being noncausal for $1 \leq y \leq 2$, power-law Green's function provides an excellent causal approximation even for observation points very close to the radiating source. For $0 < y < 2$, the Green's function decays as t^{-y+1} , leaving a slowly decaying wake behind the primary wavefront. The Green's functions reported in this paper may be used to construct solutions to diffraction and scattering problems in power-law media.

ACKNOWLEDGMENTS

The authors thank John P. Nolan, Department of Mathematics and Statistics, American University and Stephen W. Wheatcraft, Department of Geological Sciences and Engineering, University of Nevada, Reno for useful discussions and advice. Geoff Robinson, CSIRO Mathematical and Information Sciences, is also acknowledged for making his maximally skewed stable distribution code available. This work was funded in part by NIH Grant No. 1R21CA121235 and NSF Grant No. DMS-0803360.

APPENDIX A: RIEMANN-LIOUVILLE FRACTIONAL DERIVATIVES

The Riemann-Liouville fractional derivative is formally defined via a hypersingular integral⁵²

$$\frac{d^y f}{dt^y} = \frac{1}{\Gamma(-y)} \int_{-\infty}^t \frac{f(t')}{(t-t')^{1+y}} dt'. \quad (\text{A1})$$

The nonintegrable singularity is removed from Eq. (A1) by recognizing a differentiation operator, yielding

$$\frac{d^{y+1} g}{dt^{y+1}} \equiv \begin{cases} \frac{1}{\Gamma(1-y)} \frac{d^2}{dt^2} \int_0^t \frac{g(t')}{(t-t')^y} dt' & \text{if } 0 < y < 1 \\ \frac{1}{\Gamma(2-y)} \frac{d^3}{dt^3} \int_{-\infty}^t \frac{g(t')}{(t-t')^{y-1}} dt' & \text{if } 1 < y < 2. \end{cases} \quad (\text{A2})$$

In the literature, the $0 < y < 1$ case is known as the Riemann–Liouville form, whereas the $1 < y < 2$ case is the Liouville form. The following Fourier transform relationship for fractional derivatives is essential:⁵²

$$\mathcal{F}\left(\frac{d^y g}{dt^y}\right) = (-i\omega)^y \hat{g}. \quad (\text{A3})$$

In the $0 < y < 1$ case, Eq. (A3) assumes $g(t)$ vanishes for $t < 0$.

APPENDIX B: THE FOX- H FUNCTION

The Fox H -function^{20,52} is defined via a complex contour integral

$$H_{p,q}^{m,n}\left(z \left| \begin{matrix} (a_p, A_p) \\ (b_q, B_q) \end{matrix} \right. \right) \equiv \frac{1}{2\pi i} \int_L \chi(s) z^s ds, \quad (\text{B1})$$

where $(a_p, A_p) = (a_1, A_1), (a_2, A_2), \dots, (a_p, A_p)$, $(b_q, B_q) = (b_1, B_1), (b_2, B_2), \dots, (b_q, B_q)$, and the integral density $\chi(s)$ is defined as

$$\chi(s) = \frac{\prod_{j=1}^m \Gamma(b_j - B_j s) \prod_{j=1}^n \Gamma(1 - a_j + A_j s)}{\prod_{j=m+1}^q \Gamma(1 - b_j + B_j s) \prod_{j=n+1}^p \Gamma(a_j - A_j s)}. \quad (\text{B2})$$

Since the Gamma function is singular when the argument is a negative integer, Eq. (B2) contains an infinite number of poles in general. Therefore, the contour L is chosen to separate the poles of Eq. (B2). Note that Eq. (B1) is the inverse Mellin transform of Eq. (B2). The Fox H -function, which generalizes most of the special functions of mathematical physics, is discussed in great detail in Refs. 19 and 22.

APPENDIX C: THE WRIGHT FUNCTION

The Wright function $\phi(\alpha, \beta; z)$ is defined by an infinite series [see Eq. (1.11.1) in Ref. 52]:

$$\phi(\alpha, \beta; z) \equiv \sum_{k=0}^{\infty} \frac{1}{\Gamma(\alpha k + \beta) k!} z^k. \quad (\text{C1})$$

The Wright function and the more general H -function are related [see Eq. (6.2.66) in Ref. 52] via

$$H_{1,1}^{1,0}\left(z \left| \begin{matrix} (b, \alpha) \\ (0, 1) \end{matrix} \right. \right) = \phi(-\alpha, b; -z). \quad (\text{C2})$$

Equation (C2) is computed by evaluating the contour integral definition of the H -function, which possesses an infinite

number of poles, with Cauchy's residue theorem. The resulting infinite series is identified as Eq. (C1).

- ¹F. A. Duck, *Physical Properties of Tissue*, 1st ed. (Academic, London, 1990), pp. 99–124.
- ²M. J. Buckingham, "Causality, Stokes' wave equation, and acoustic pulse propagation in a viscous fluid," *Phys. Rev. E* **72**, 026610 (2005).
- ³P. M. Morse and H. Feshbach, *Methods of Theoretical Physics* (McGraw-Hill, New York, 1953).
- ⁴T. L. Szabo, "Time-domain wave-equations for lossy media obeying a frequency power-law," *J. Acoust. Soc. Am.* **96**, 491–500 (1994).
- ⁵A. Hanyga and M. Seređyńska, "Power-law attenuation in acoustic and isotropic anelastic media," *Geophys. J. Int.* **155**, 830–838 (2003).
- ⁶M. Caputo, "Linear models of dissipation whose Q is almost frequency independent-II," *Geophys. J. R. Astron. Soc.* **13**, 529–539 (1967).
- ⁷M. G. Wismer, "Finite element analysis of broadband acoustic pulses through inhomogeneous media with power law attenuation," *J. Acoust. Soc. Am.* **120**, 3493–3502 (2006).
- ⁸W. Chen and S. Holm, "Fractional Laplacian time-space models for linear and nonlinear lossy media exhibiting arbitrary frequency power-law dependency," *J. Acoust. Soc. Am.* **115**, 1424–1430 (2004).
- ⁹R. Schumer, D. A. Benson, M. M. Meerschaert, and S. W. Wheatcraft, "Eulerian derivation of the fractional advection-dispersion equation," *J. Contam. Hydrol.* **48**, 69–88 (2001).
- ¹⁰S. Leeman, "Ultrasound pulse propagation in dispersive media," *Ultrasound Med. Biol.* **25**, 481–488 (1980).
- ¹¹J. M. Blackledge and S. Leeman, "Green's functions for acoustic fields in dispersive media," *J. Phys. D: Appl. Phys.* **16**, L247–L250 (1983).
- ¹²M. O'Donnell, E. T. Jaynes, and J. G. Miller, "Kramers–Krönig relationship between ultrasonic attenuation and phase velocity," *J. Acoust. Soc. Am.* **69**, 696–701 (1981).
- ¹³T. L. Szabo, "Causal theories and data for acoustic attenuation obeying a frequency power-law," *J. Acoust. Soc. Am.* **97**, 14–24 (1995).
- ¹⁴K. R. Waters, M. S. Hughes, J. Mobley, G. H. Brandenburger, and J. G. Miller, "On the applicability of Kramers–Krönig relations for ultrasonic attenuation obeying a frequency power law," *J. Acoust. Soc. Am.* **108**, 556–563 (2000).
- ¹⁵K. V. Gurusurthy and R. M. Arthur, "A dispersive model for the propagation of ultrasound in soft tissue," *Ultrason. Imaging* **4**, 355–377 (1982).
- ¹⁶T. L. Szabo, "The material impulse response for broadband pulses in lossy media," *Proceedings of the IEEE Ultrasonics Symposium, Honolulu, HI 2003* (unpublished), pp. 741–751.
- ¹⁷P. He, "Simulation of ultrasound pulse propagation in lossy media obeying a frequency power law," *IEEE Trans. Ultrason. Ferroelectr. Freq. Control* **45**, 114–125 (1998).
- ¹⁸N. V. Sushilov and R. S. Cobbold, "Frequency-domain wave equation and its time-domain solutions in attenuating media," *J. Acoust. Soc. Am.* **115**, 1431–1436 (2004).
- ¹⁹A. M. Mathai and R. K. Saxena, *The H-function with Applications in Statistics and Other Disciplines* (Wiley, New York, 1978).
- ²⁰R. Gorenflo, Y. Luchko, and F. Mainardi, "Analytical properties and applications of the Wright function," *Fractional Calculus Appl. Anal.* **2**, 383414 (1999).
- ²¹R. Gorenflo and F. Mainardi, "Fractional calculus and stable probability distributions," *Arch. Mech.* **50**, 377–388 (1998).
- ²²W. G. Glöckle and T. F. Nonnenmacher, "Fox function representation of non-Debye relaxation processes," *J. Stat. Phys.* **71**, 741–756 (1993).
- ²³M. Liebler, S. Ginter, T. Dreyer, and R. E. Riedlinger, "Full wave modeling of therapeutic ultrasound: Efficient time-domain implementation of the frequency power-law attenuation," *J. Acoust. Soc. Am.* **116**, 2742–2750 (2004).
- ²⁴D. T. Blackstock, "Transient solution for sound radiated into a viscous fluid," *J. Acoust. Soc. Am.* **41**, 1312–1319 (1967).
- ²⁵D. G. Crighton, *Modern Methods in Analytical Acoustics: Lecture Notes* (Springer-Verlag, London, 1996).
- ²⁶J. F. Kelly and R. J. McGough, "The causal impulse response for circular sources in viscous media," *J. Acoust. Soc. Am.* **123**, 2107–2116 (2008).
- ²⁷R. S. C. Cobbold, N. V. Sushilov, and A. C. Weathermon, "Transient propagation in media with classical or power-law loss," *J. Acoust. Soc. Am.* **116**, 3294–3303 (2004).
- ²⁸G. Samorodnitsky and M. Taqqu, *Stable Non-Gaussian Random Processes* (Chapman and Hall, New York, 1994).
- ²⁹J. P. Nolan, *Stable Distributions: Models for Heavy Tailed Data* (Birkhauser, New York, 2005).

- ³⁰W. Feller, *An Introduction to Probability Theory and Its Applications* (Wiley, New York, 1966), pp. 165–173, and 548–549.
- ³¹V. M. Zolotarev, *One-Dimensional Stable Distributions* (American Mathematical Society, Providence, RI, 1986).
- ³²J. P. Nolan, “Numerical calculation of stable densities and distribution functions,” *Commun. Stat. Stoch. Models* **13**, 759–774 (1997); <http://academic2.american.edu/~jpholan/stable/stable.html>
- ³³M. Kanter, “Stable densities under change of scale and total variation inequalities,” *Ann. Probab.* **3**, 697–707 (1975).
- ³⁴H. Pollard, “The representation of e^{-z^λ} as a Laplace integral,” *Bull. Am. Math. Soc.* **52**, 908–910 (1946).
- ³⁵M. Dishon, J. T. Bendler, and G. H. Weiss, “Tables of the inverse Laplace transform of the function e^{-s^β} ,” *J. Res. Natl. Bur. Stand., Sect. B* **95**, 433–467 (1990).
- ³⁶A. Hanyga and V. E. Rok, “Wave propagation in micro-heterogeneous porous media: A model based on an integral-differential wave equation,” *J. Acoust. Soc. Am.* **107**, 2965–2972 (2000).
- ³⁷A. Hanyga, “Propagation of pulses in viscoelastic media,” *Pure Appl. Geophys.* **159**, 1749–1769 (2002).
- ³⁸W. R. Schneider, “Stable distributions: Fox function representation and generalization,” in *Stochastic Processes in Classical and Quantum Systems*, edited by S. Albeverio, G. Casati, and D. Merlini (Spring-Verlag, Berlin, 1985).
- ³⁹F. Mainardi and G. Pagnini, “The Wright functions as solutions of the time-fractional diffusion equation,” *Appl. Math. Comput.* **141**, 51–62 (2003).
- ⁴⁰R. Metzler, W. G. Glöckle, and T. F. Nonnenmacher, “Fractional model equation for anomalous diffusion,” *Physica A* **211**, 13–24 (1994).
- ⁴¹T. Kobayashi and S. Imai, “Spectral analysis using generalized cepstrum,” *IEEE Trans. Acoust., Speech, Signal Process.* **32**, 1087–1089 (1984).
- ⁴²M. Galassi, *GNU Scientific Library Reference Manual*, 2nd ed. (Network Theory Ltd., Bristol, UK, 2006).
- ⁴³G. Robinson, “Rapid computations concerning log maximally-skewed stable distributions, with potential use for pricing options and evaluating portfolio risk,” Private Report, 2005.
- ⁴⁴N. Denisenko, G. Scarano, M. Matteucci, and M. Pappalardo, “An approximate solution of the transient acoustic field,” *IEEE Trans. Ultrason. Ferroelectr. Freq. Control* **46**, 821–827 (1985).
- ⁴⁵J. L. San Emeterio and L. G. Ullate, “Diffraction impulse-response of rectangular transducers,” *J. Acoust. Soc. Am.* **92**, 651–662 (1992).
- ⁴⁶J. A. Jensen, D. Gandhi, and W. D. O’Brien, “Ultrasound fields in an attenuating medium,” *Proceedings of the IEEE Ultrasonics Symposium*, Baltimore, MD, 1993, pp. 943–946.
- ⁴⁷G. Pinton and G. Trahey, “Full-wave simulation of finite-amplitude ultrasound in heterogeneous media,” *Proceedings of the IEEE Ultrasonics Symposium*, New York, 2007, pp. 130–133.
- ⁴⁸J. F. Kelly and R. J. McGough, “Transient acoustic fields produced by rectangular apertures and linear arrays in viscous media,” *Proceedings of the IEEE Ultrasonics Symposium*, New York, 2007, pp. 1553–1556.
- ⁴⁹B. Baeumer, D. A. Benson, M. M. Meerschert, and S. W. Wheatcraft, “Subordinated advection-dispersion equation for contaminant transport,” *Water Resour. Res.* **37**, 1543–1550 (2001).
- ⁵⁰J. M. Collis, W. M. Carey, and A. D. Pierce, “A physical explanation for less than quadratic recorded attenuation values,” *OCEANS 2007 Europe*, Aberdeen, Scotland, 18–21 June 2007, pp. 1–3.
- ⁵¹T. L. Szabo, *Diagnostic Ultrasound Imaging: Inside Out* (Elsevier Academic, Burlington, MA, 2004).
- ⁵²A. A. Kilbas, H. M. Srivastava, and J. J. Trujillo, *Theory and Applications of Fractional Differential Equations* (Elsevier, Amsterdam, 2006).